Chapter

Challenges and Strategies of High-Capacity Transition Metal Oxides as Anodes for Lithium-Ion Batteries (LIBs)

Loubna Hdidou, Fouad Ghamouss, Bouchaib Manoun, Hassan Hannache, Jones Alami and Mouad Dahbi

Abstract

To satisfy the growing demand for high-energy and high-power-densities Lithium-ion Batteries (LIBs), the design and development of efficient electrode materials are necessary. In comparison to graphite, transition metal oxides (TMOs) have recently been widely investigated as anode materials due to their promising properties. These combine high specific capacities and high working potential, making them attractive anode candidates for emergent applications. Unfortunately, because of their poor electronic conductivity and high-volume expansion during cycling, they are unpractical and difficult to employ. To overcome these limitations, different approaches have been adopted. Examples are synthesizing the metal oxides at the nanometric scale, designing three-dimensional or hollow structures, coating the material with carbonaceous materials, etc. In this chapter, we report the elaboration of nanostructured transition metal oxides (Co_3O_4, Mn_3O_4, $Co_{3-x}Mn_xO_4$) using alginate gelling synthesis method. The Co_3O_4 octahedral-like nanoparticles display a remarkable cycling performance and good rate capability of 1194 mAh g^{-1} at C/5 and 937 mAh g^{-1} at 2C. Partially substituting the Co with Mn was shown to result in the production of $Co_{2.53}Mn_{0.47}O_4$ and $MnCo_2O_4$ with high initial specific discharge capacities of 1228/921 and 1290/954 mAh g^{-1}, respectively. As a Co-free material, the Mn_3O_4 delivers a reversible capacity of 271 mAh g^{-1}, after 100 cycles.

Keywords: lithium-ion batteries, transition metal oxides, high-capacity, anode materials, alginate gelling method

1. Introduction

Since their commercialization, (LIBs) have been regarded as the most efficient energy storage system. They have been integrated into portable electronics and electrical devices. Their energy density has increased gradually until ~250Wh kg^{-1} [1]. The LIBs operating mechanism is based on the lithium-ion exchange between the

cathode and the anode materials. During the charging process, an external current is applied to the cell, forcing the lithium-ion to leave the cathode moving to the anode. Inversely, during the discharge, which is a spontaneous reaction, the lithium-ion is transferred from the anode to the cathode. To preserve electrical neutrality, electrons are also transported to the cathode through an external circuit. Then, the electrical energy that was stored as chemical energy during the charging process is produced. The conversion of the chemical energy to electrical energy and vice-versa is based on the redox reaction of metallic elements present at the electrodes. These reactions are controlled by the chemical potential difference. The LIBs performances depend mainly on the combination of their different constituents, including the positive and negative electrodes, the electrolyte, and the separator.

The anode material is one of the critical components of the LIBs and depending on the Li^+ ion reaction with the active material, three different storing mechanisms could be listed. These are the intercalation, the alloying, and the conversion. Graphite is considered the most employed negative electrode material for LIBs [2]. Its working mechanism is based on the Li^+ intercalation/deintercalation into the graphite interlayer, following the reaction: $6C + xLi^+ + xe^{-1} \leftrightarrow Li_xC_6$ [2]. With a theoretical capacity of 372 mAh g^{-1}, the graphite anode delivers a capacity that is higher than 360 mAh g^{-1} and shows good reaction reversibility. Nonetheless, due to its low capacity, other carbonaceous materials were examined, such as graphene [3], hollow spheres, nanotubes [4], nanofibers [5], porous materials, etc. For graphene and hollow carbon spheres, it was demonstrated that the Li^+ storage took place due to the surface adsorption and the interactions with the carbon functional groups [6, 7].

Non-carbonaceous materials were also tested as anode materials for LIBs. Alloying elements such as Si, Ge, and Sn are considered promising alternatives. Particularly, Si exhibits the highest gravimetric capacity of 4200 mAh g^{-1} [8]. The lithiation mechanism happens in two steps, the first one where the $Li_{13}Si_4$ alloy is formed, and the second consists of the formation of $Li_{22}Si_5$ phase [9]. Ge and Sn also show high initial theoretical capacities of 1600 mAh g^{-1} and 993 mAh g^{-1}, respectively [10, 11].

Metal oxides are a very attractive class of materials, they are regarded as one of the most intriguing alternative graphite materials because of their high specific capacities and high working potential. Recently different oxides, such as Fe_2O_3 [12], MnO [13], NiO [14], Mn_3O_4 [15], $CoFe_2O_4$, $MnFe_2O_4$ and $NiFe_2O_4$ [16, 17] were used as anodes. They are generally known to react with lithium by a conversion reaction, where the metal ions are reduced to metallic form and then oxidized during consecutive discharge/charge operations:

$$M_aO_b + (b.n)Li^+ + (b.n)e^- \leftrightarrow aM + bLi_nO \quad (1)$$

Where M=Mn, Fe, Co, Ni, Cu, Ru, Mo, Cr, W, etc.

The In-situ transmission electron microscopy (TEM) technique demonstrates that the lithiation process of metal oxides occurs first via an intercalation reaction with the formation of metastable and intermediate phases, followed by a conversion reaction [18]. During a discharge process, with a metallic lithium counter electrode, the metallic cations are reduced to their nanometric metallic elements and get surrounded by Li_2O which is chemically more stable than any other metal oxide. However, when lithium-ion is electrochemically extracted from the composite (charge), the metallic species clusters get disintegrated and converted to small, dispersed particles with a high active specific surface area. This increases oxygen contact and catalyzes the formation of the metallic oxides as Li_2O decomposes. The charge process involves

the deconversion of the metallic species formed during the discharge process and the decomposition of the inactive lithium oxide Li_2O by cleaving the stable Li-O bonds.

Even if metal oxides exhibit high-capacity values, they have been known to suffer from important volume expansion reaching up to 200% during the lithiation process. This induces the electrode's pulverization and disintegration, resulting in the loss of particle contact, a take-off from the current collector, and the formation/deformation of a solid electrolyte interface (SEI) layer, leading to an acceleration of capacity drop [19–21]. To improve the metal oxides cyclability different approaches have been adopted [22, 23].

2. Engineering approaches for high performances transition metal oxides

2.1 Design of three-dimensional (3D) structures or hierarchical configurations

Three-dimensional (3D) structures or hierarchical configurations are generally built from 0D, 1D, or 2D particles resulting in structures with enhanced porosity and relatively large specific surface areas. Three-dimensional structures have several advantages; they provide more channels for Li^+ and e^- diffusion, a larger electrode/electrolyte contact area, and improved stress resistance to volume change during the Li^+ insertion/extraction [21]. A 3D structure made of vertical nanowires of Co_3O_4 with an improved electrical conductivity was prepared by Wang et al. The Co_3O_4 shows stable cycling and a high coulombic efficiency of around 100%. When assembled in a full cell system with lithium iron phosphate, LFP, cathode, the cell exhibits a capacity of 138 mAh g^{-1} with a capacity retention of 96% after 100 cycles [24]. Kong et al. reported the elaboration of 3D hierarchical $MnCo_2O_4$ porous dumbbells exhibiting a stable reversible capacity of 955 mAh g^{-1} after 180 cycles at 200 mA g^{-1} [25]. Hierarchical conversion metal oxides have also stimulated efforts for the development of binder-free negative electrodes for the next-generation LIBs. In a recent study, Wu et al. have reported the elaboration of self-supporting multilevel-3D porous NiO nanowires as a binder-free anode material. The synthesized NiO displayed superior electrochemical performances, with a specific capacity that reached 1816.3 mAh g^{-1} at the current density of 100 mA g^{-1}, and remained at 1318.7 mAh g^{-1} after 150 cycles [26].

2.2 Design of nanoparticles

As an anode for lithium-ion batteries, nanoparticles display superior properties compared to their bulk counterparts. Their reduced size significantly increases the Li-ion diffusion rate. We recall that the characteristic diffusion time constant is given by the equation:

$$\hat{o}_{eq} = L^2 / D \tag{2}$$

where L is the diffusion length and D is the diffusion constant.

Recognizing that the mean diffusion time (τ_{eq}) is proportional to the square of the diffusion length (L), it is safe to claim that when the particle size is reduced, the intercalation time decreases. The nanoparticles' high specific surface area provides more electroactive sites and displays an important contact area with the electrolyte [20]. Recently, a variety of nano-sized metal oxides such as Mn_2O_3 [27], Co_3O_4 [28], Fe_3O_4 [29], etc. have been reported.

2.3 Design of hollow structures

A hollow structure is another alternative to enhance electrochemical properties. It is attracting increasing attention because of its ability to buffer the volume expansion during the cycling process and to increase the contact between the inner active material and the electrolyte due to the presence of voids inside these structures. Jian et al. have prepared Mn_3O_4 hollow spheres, using an aerosol-based "droplet to particle" method and evaluated them as anode material in LIBs. The particles displayed capacity retention of ~980 mA g^{-1} for over 140 cycles at 200 mA g^{-1} [30]. Hollow $CoFe_2O_4$@Fe_3O_4 nanospheres have also shown good cycling stability, after 500 cycles, with a specific capacity of 365 mAh g^{-1} at a current density of 1000 mA g^{-1} [31]. Xie et al. have reported the elaboration of hollow Fe_3O_4/rGO composites with a reversible capacity of 827.3 mAh g^{-1} after 550 cycles at 0.5 A g^{-1} [32].

2.4 Carbon coating and hybridization with carbonaceous materials

To enhance the electronic conductivity and the reaction kinetics during cycling, metal oxide particles are coated with carbon. Alternatively, they are inserted into a carbonaceous matrix. In both cases, the strain of volume change during the Li^+ ion insertion/extraction is better accommodated, and particles aggregation is avoided. A carbon shell can be also an effective barrier between the electrode and the electrolyte, which stabilizes the solid electrolyte interface and prevents electrolyte decomposition. Different studies have synthesized hybrid metal oxide/carbon materials as high-efficiency anodes for advanced lithium-ion batteries.

To produce $CoFe_2O_4$/C fibers, Wu et al. used the electrospinning technique. The $CoFe_2O_4$/C composite was evaluated for its performance as an anode, demonstrating a reversible capacity of 490 mAh g^{-1} after 700 cycles [33]. In a different study, Li et al. reported on the elaboration of $CoFe_2O_4$ nanoparticles, uniformly dispersed, on graphene sheets. This three-dimensional (3D) network exhibited a specific reversible capacity of up to 938 mAh g^{-1}, at a current density of 1000 mA g^{-1} [34]. Nitrogen-doped porous Carbon/Co_3O_4 nanocomposites were obtained via a hydrothermal method using natural porous crawfish shells as the carbon source. This composite delivered an irreversible discharge capacity of 1060 mAh g^{-1} at a current density of 100 mA g^{-1} [35].

In this chapter, we report the synthesis of Co_3O_4, Mn_3O_4, $Co_{2.53}Mn_{0.47}O_4$, and $MnCo_2O_4$ at the nanometric scale for use as anode materials for LIBs, by a bio-inspired simple synthesis method, using alginate biopolymer as a bio-template for crystals nucleation and growth.

3. Design of nanostructured Co_3O_4, Mn_3O_4, $Co_{2.53}Mn_{0.47}O_4$, and $MnCo_2O_4$ as high-performance anode materials for the next generation LIBs

3.1 Nanostructured Co_3O_4 as anode material for LIBs

Following a synthesis procedure by Hdidou et al. [36], Co_3O_4 was prepared via the alginate gelling method. A sodium alginate aqueous solution was prepared under medium stirring at room temperature. Subsequently, hydrogel beads were formed by adding, dropwise, the obtained solution into a homogeneous metal solution containing Co^{2+} cations. The beads were gently stirred in the metal solution overnight before

filtration, washing with distilled water, and drying. The sacrificial bio-template was removed by heating the xerogels in airflow at 600°C.

During the synthesis process, the alginate biopolymer could be used as:

- A stabilizer to control the particle size and the specific surface area;
- A template to direct the structure and the morphology of particles;
- An Oxygen donor.

The powder X-ray diffraction (XRD) patterns of the Co-alginate composite obtained after the thermal treatment, confirm the formation of the cubic spinel structure Co_3O_4 with a *Fd-3m* space group (**Figure 1**). The synthesized material's morphology and particle size were characterized by Scanning Electron Microscopy (SEM), as shown in **Figure 2**. The images reveal the presence of polyhedral octahedral-like nanoparticles with a heterogeneous particle size distribution and an average size of 90 nm. The particles exhibit a Brunauer–Emmett–Teller (BET) specific surface area of 12.4 m^2g^{-1}. The morphology and the particle size are relevant parameters that have a direct impact on a material's electrochemical properties. One of the most effective methods to improve electrode kinetics is the elaboration of the active material at the nanometric scale. Generally, nanoparticles provide a huge electrode/electrolyte contact area, a reduced distance for Li^+ diffusion and electron transfer, and more electro-active sites.

To evaluate the electrochemical performance of the nanostructured Co_3O_4 electrode, cyclic voltammetry (CV) and galvanostatic tests were performed. The cyclic voltammetry curve of Co_3O_4 is illustrated in **Figure 3b**. It is seen that during the first scan of Co_3O_4, the main reduction peak is located at 0.66 V and is attributed to the reduction of Co^{3+} and Co^{2+} to Co, and the formation of the solid-electrolyte-interface (SEI) layer. The main oxidation peak was observed at 2.07 V and is associated with the oxidation reaction of Co/Co_3O_4. The proposed Li^+ storage mechanism is according to the following reaction [37]:

$$Co_3O_4 + 8Li^+ + 8e- \leftrightarrow 3Co + 4Li_2O \quad (3)$$

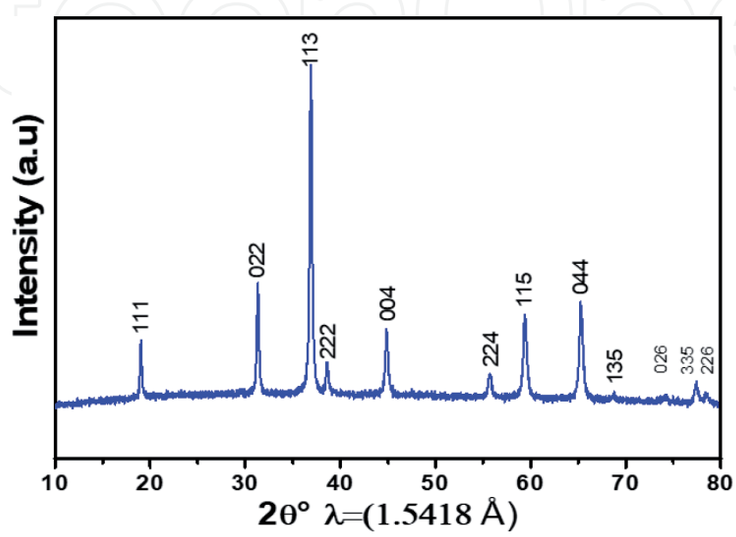

Figure 1.
X-ray powder diffraction patterns of Co_3O_4.

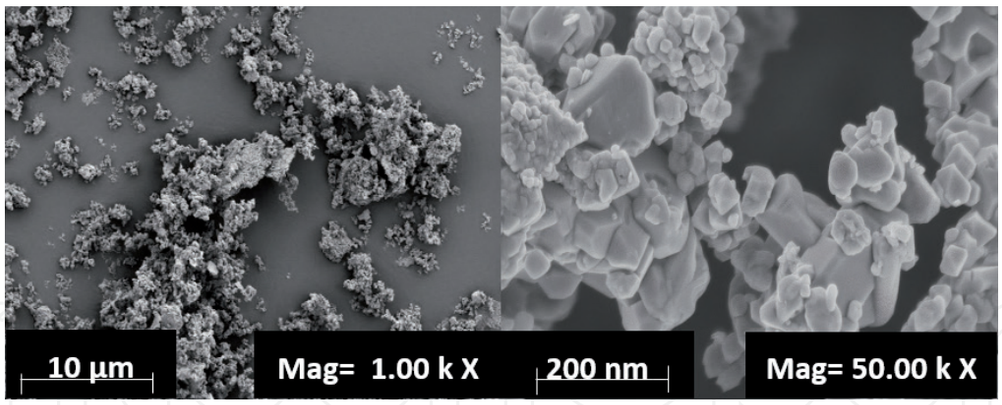

Figure 2.
SEM images of Co_3O_4.

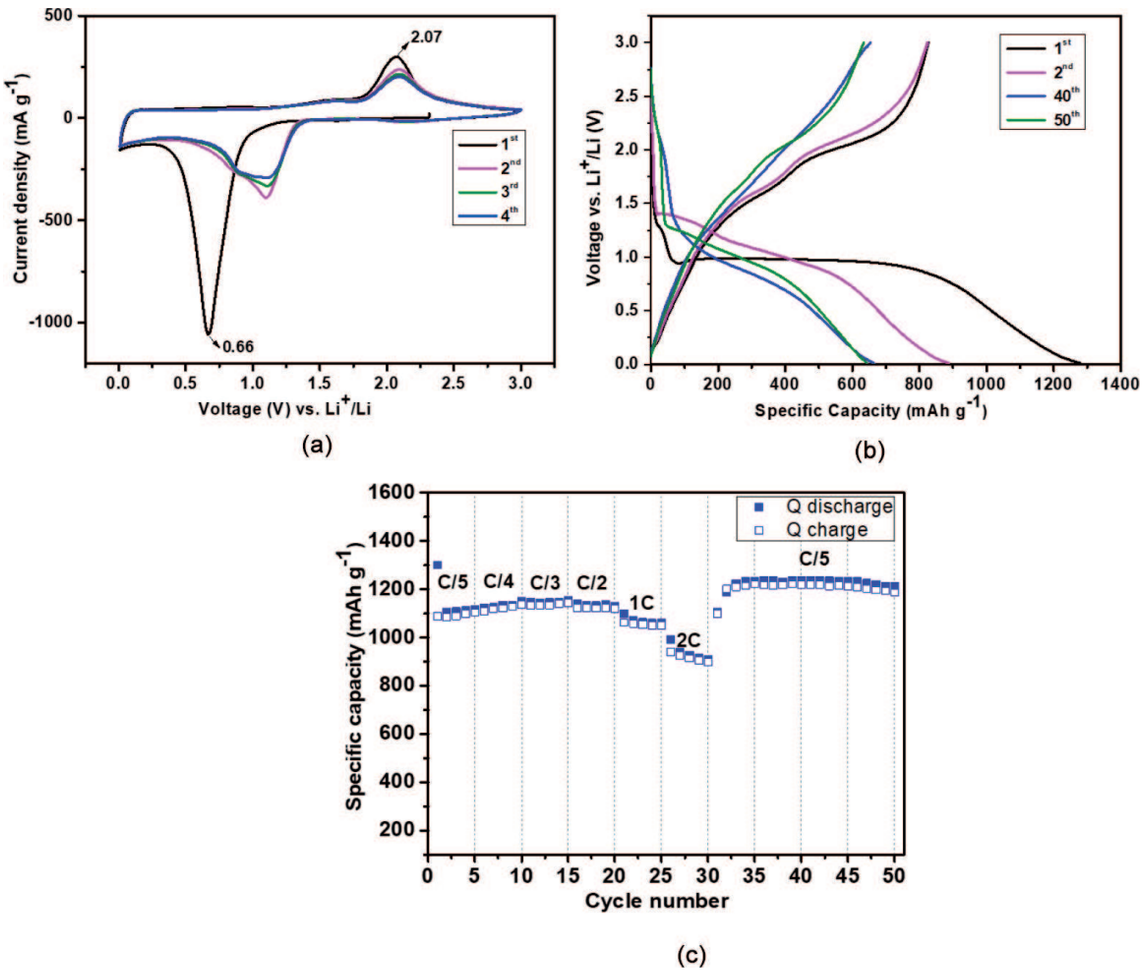

Figure 3.
Electrochemical performances of Co_3O_4 (a) Cyclic voltammogram of the as-prepared Co_3O_4 in the voltage range of 0.01–3.00 V vs. Li/Li^+ at a scan rate of 0.05 mV s^{-1}, (b) Charge-discharge profiles of Co_3O_4 at the current rate of C/5 in the voltage range of 0.01–3.00 V (c) Rate capability of Co_3O_4 electrode material at various current rates from C/5 to 2C.

Further investigation showed that the shape of the CV curve is mostly maintained in the subsequent sweeps, indicating good cycle reversibility of the electrochemical reactions [38, 39]. Starting from the second cycle, the CV curves display overlapped two reduction peaks located at around 1.1 and 0.91 V, assigned to the reversible reduction of Co^{3+} to Co^{2+} and Co^{2+} to Co, respectively. These peaks become

broader with lower intensities compared to the first cycle which is due to the pseudo-capacitive behavior of the metal oxide that starts taking place during the following cycles due to the particle size reduction and the irreversible Co and Mn elements formation, indicating the capacity loss. **Figure 3a** displays the galvanostatic charge/discharge performances of the Co_3O_4 electrode, examined at a C/5 current rate in the voltage window of 0.01–3.00 V (1C = 1.23 A g^{-1}). The electrode delivers a high initial specific discharge capacity of 1008 mAh g^{-1} with a coulombic efficiency (CE) of 75%. After 50 cycles the capacity was maintained to 680 mAh g^{-1} with a CE of 99%. During the first discharge curve, a large discharge plateau at 1.06 V appeared, corresponding to the lithium reaction with Co_3O_4 and the formation of SEI. During charging, a plateau was also observed at 1.9 V. This plateau is attributed to a Co/Co_3O_4 oxidation reaction during the lithium-ion extraction process (**Figure 3b**). The enhanced electrochemical performance of Co_3O_4 could be attributed to the reduced particle size of 90 nm and the reactions reversibility during the lithiation/delithiation process. As was expected from the galvanostatic test, Co_3O_4 exhibits good rate capability performances. The cell delivers average specific discharge capacities of 1149, 1133, 1147, 1134, 1070, and 937 mAh g^{-1}, with coulombic efficiencies of 95, 97, 91, 98, 99, and 97% at the current rate of C/5, C/4, C/3, C/2, 1C, and 2C respectively. When the current density was set back to C/5, a high specific discharge capacity of 1222 mAh g^{-1} was recovered with a CE of 96%. Indicating its tolerance to the fast Li^+ lithiation/delithiation process (**Figure 3b**).

3.2 Nanostructured $Co_{3-x}Mn_xO_4$ (x = 0.47, 1) as anode materials for LIBs

The insertion of the Mn into the Co_3O_4 structure was ensured using the alginate gelling synthesis method. The alginate solution was added drop by drop into a homogeneous metal solution containing a mixture of Co^{2+} and Mn^{2+} cations. The obtained gel was then washed, dried, and calcined under an air atmosphere. The substitution of Co^{3+} (0.54 Å) by Mn^{3+} (0.58 Å) cations that have a larger ionic radius was confirmed by the X-ray diffraction (**Figure 4**) and the atomic absorption spectroscopy analysis. $Co_{2.53}Mn_{0.47}O_4$ and $MnCo_2O_4$, with cubic spinel structures adopting *Fd-3m* as a space group, have been produced. Analysis of the SEM images showed that $Co_{3-x}Mn_xO_4$ (x = 0.47, 1) crystallizes into an octahedral-like morphology since the growth of nanoparticles is privileged along the axis <100>. The average particle size calculated by ImageJ software of $Co_{2.53}Mn_{0.47}O_4$ and $MnCo_2O_4$ is 72 and 69 nm respectively (**Figure 5**). Using a scanning electron microscope, coupled with an energy-dispersive X-ray spectroscope (EDS), the elemental composition revealed the presence of Co and Mn as the major elements. This is shown in **Figure 6** where other elements such as Na, and Ca could also be detected.

The mixed oxides $Co_{3-x}Mn_xO_4$ (x = 0.47, 1), demonstrate a promising electrochemical activity with high specific discharge capacities of 1228 and 1290 mAh g^{-1} and an initial CE of 75 and 74% (**Figure 7a** and **b**). This capacity could not be maintained in long-term cycling, which was also observed by Lai et al., who reported that with increasing the cycle numbers the Mn element gets dissolved into the electrolyte and settles down on the electrode surface [40]. From the cyclic voltammetry profile, the two cathodic peaks were observed during the conversion reaction for each compound (1.21 V/0.70 V, and 1.28 V/0.62 V), they are assigned to the reduction process of Mn/Mn^{3+} and Co/Co^{3+}, respectively. However, three of the observed anodic peaks, 2.09/1.52/1.10 V, 2.01/1.52/1.13 V, could be attributed to the oxidation of Co to Co^{2+} and Co^{3+}, and Mn to Mn^{2+} [41] (**Figure 7c** and **d**).

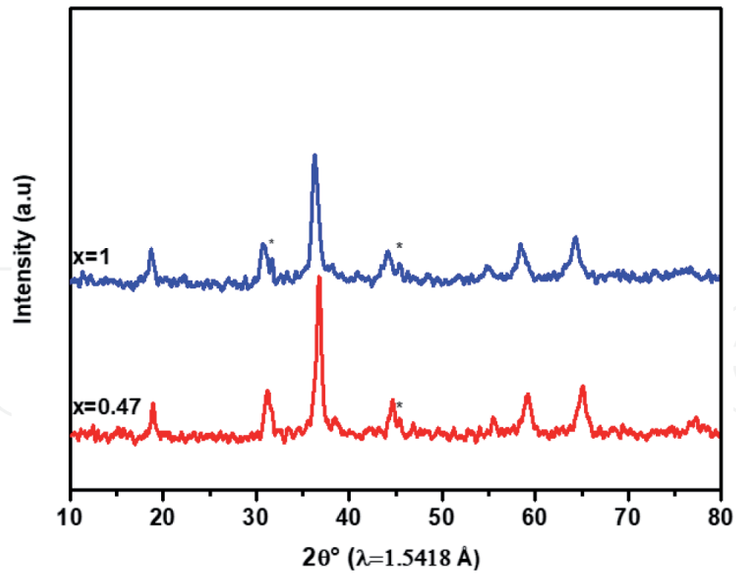

Figure 4.
X-ray powder diffraction patterns of $Co_{2.53}Mn_{0.47}O_4$ and Co_2MnO_4.

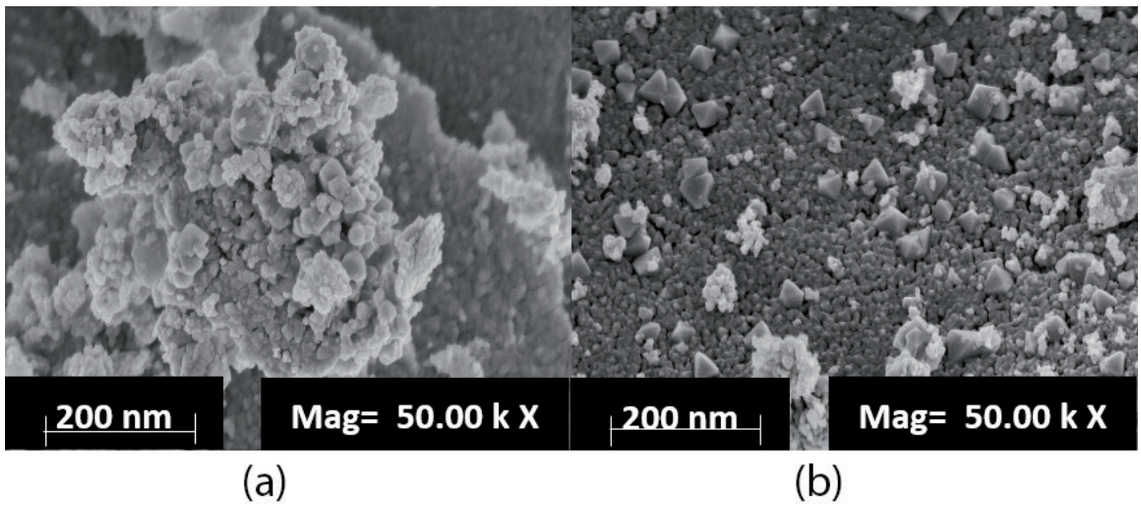

Figure 5.
SEM images of the synthesized oxides (a) $Co_{2.53}Mn_{0.47}O_4$ and (b) Co_2MnO_4.

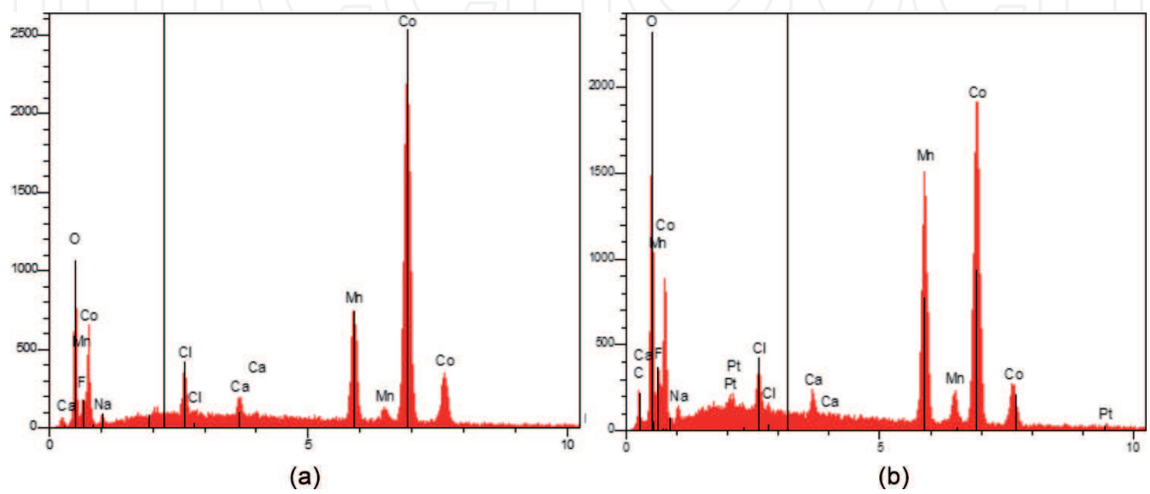

Figure 6.
EDS analysis of the synthesized oxides (a) $Co_{2.53}Mn_{0.47}O_4$ and (b) Co_2MnO_4.

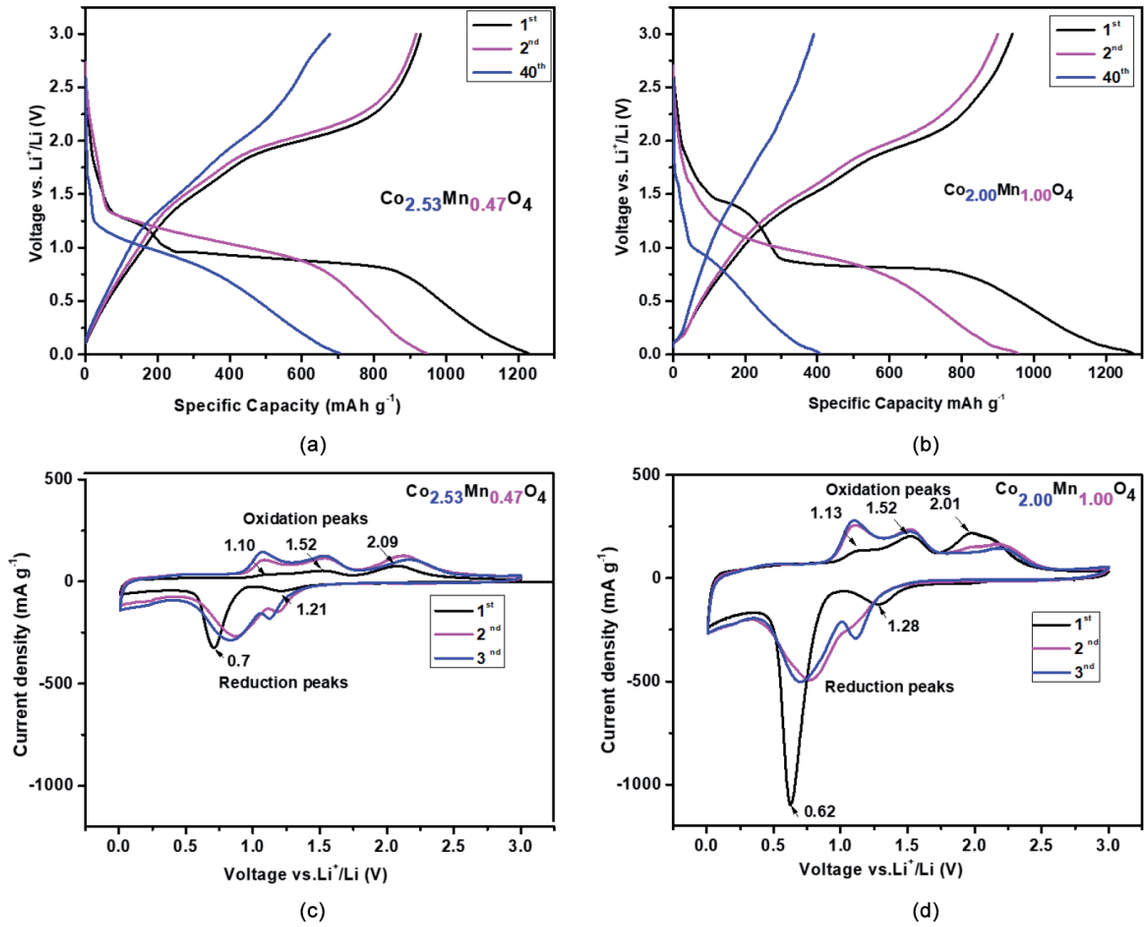

Figure 7.
Electrochemical performances of $Co_{2.53}Mn_{0.47}O_4$ and Co_2MnO_4 (a, b) Charge-discharge profiles of $Co_{2.53}Mn_{0.47}O_4$ and Co_2MnO_4 at the current rate of C/5 in the voltage range of 0.01–3.00 V (c, d) Cyclic voltammograms of the as-prepared $Co_{2.53}Mn_{0.47}O_4$ and Co_2MnO_4 in the voltage range of 0.01–3.00 V vs. Li/Li^+ at a scan rate of 0.05 mV s^{-1}.

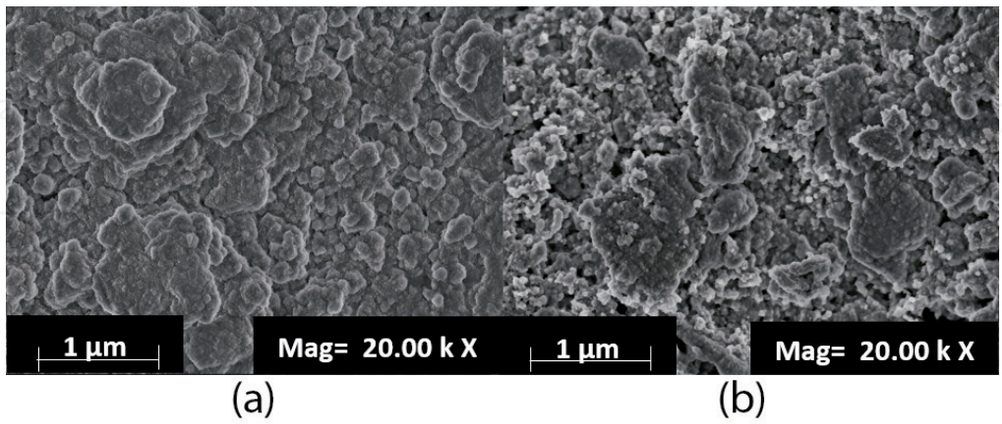

Figure 8.
SEM images of the electrodes (a) $Co_{2.53}Mn_{0.47}O_4$, and (b) Co_2MnO_4, after 2 cycles.

The particle morphology was also examined. **Figure 8a** and **b** revealed that after two cycles, the nanometric size distribution was retained and the structure was still observed. Nonetheless, a thin layer was formed on the electrode surface. It refers to the SEI films that originated from the decomposition of the electrolyte and the consumption of salt, and solvent species [42].

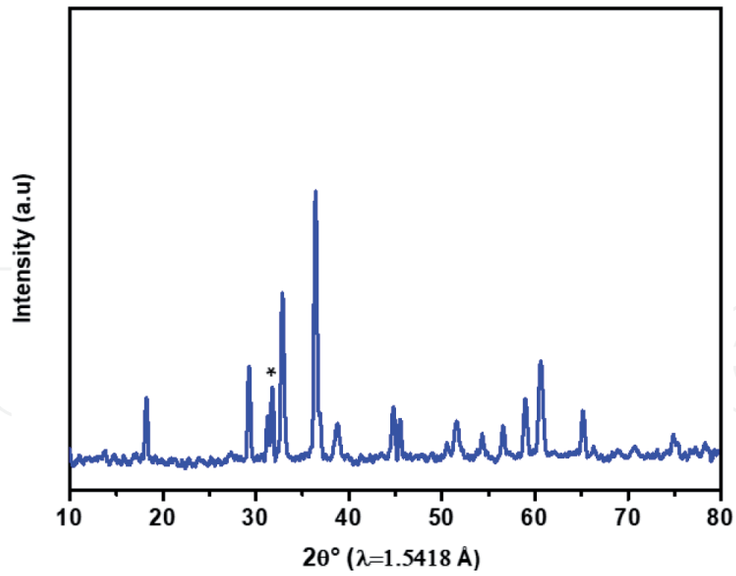

Figure 9.
X-ray powder diffraction patterns of Mn_3O_4.

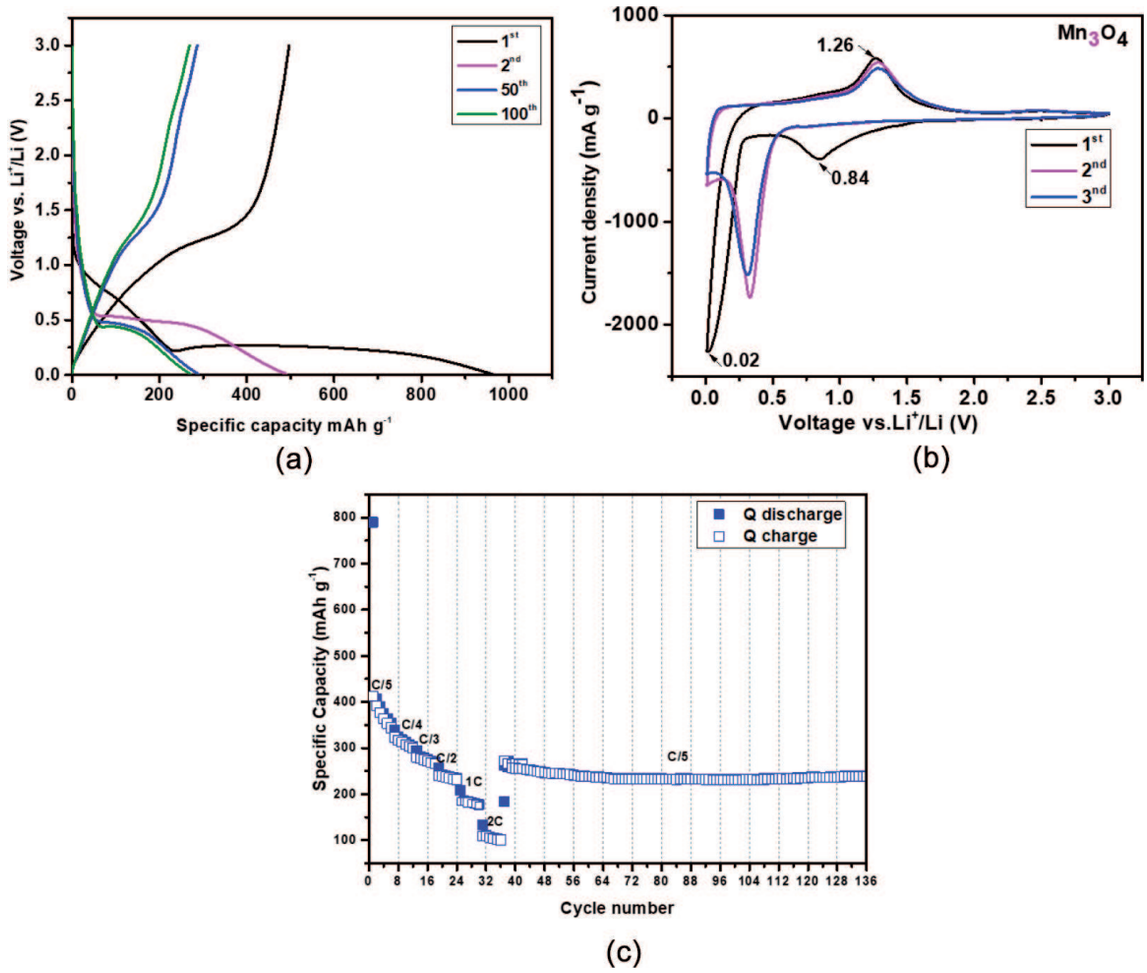

Figure 10.
Electrochemical performances of Mn_3O_4 (a) Charge-discharge profiles of Mn_3O_4 at the current rate of C/5 in the voltage range of 0.01–3.00 V, (b) Cyclic voltammogram of the as-prepared Mn_3O_4 in the voltage range of 0.01–3.00 V vs. Li/Li^+ at a scan rate of 0.05 mV s^{-1}, (c) Rate capability of Mn_3O_4 electrodes material at various current rates from C/5 to 2C.

3.3 Nanostructured Mn_3O_4 as anode material for LIBs

The elaboration of Mn_3O_4 by the alginate gelling method is also reported in this chapter. The Mn_3O_4 spinel oxide was produced by calcining the hybrid Mn-alginate xerogel at 600 °C under the air atmosphere. This phase adopts *I*41/*amd* as a space group. Mn_3O_4 is a tetragonal distorted spinel with an ionic structure of $Mn^{2+}\left[Mn_2^{3+}\right]O_4$, where Mn^{2+} are located in the tetrahedral sites and Mn^{3+} in the octahedral sites. The sample shows an impurity peak which was indexed as Mn_5O_8 (**Figure 9**).

As a free Co material, Mn_3O_4 shows moderate electrochemical performance. The initial specific discharge/charge capacities delivered by the prepared material are 960, 497 mAh g^{-1} with a CE of 51%. Between the first and the second cycle, the discharge capacity drops to its half. Nevertheless, between the 50th and 100th cycles, only a loss of 14 mAh g^{-1} was observed and a capacity of 271 mAh g^{-1} was maintained (**Figure 10a**). With increasing the cycle number, the specific capacity gets more stable. This stability could be attributed to the activation process resulting from the increase of the lithium-ion reactivity with the appearance of Mn^{2+}/Mn^{4+} redox reaction [25]. The coulombic efficiency rises to 98.9% indicating its good capacity retention. At the first discharge curve, a pseudo-plateau at 0.70 V with a large plateau at 0.24 V took place, which is related to the lithium insertion reactions and the electrolyte decomposition (**Figure 10a**). From the CV test, in the first cathodic scan, the broad peak at 0.30 V is attributed to the reduction of Mn^{3+} into Mn^{2+} and the formation of a solid-electrolyte-interface (SEI) layer (peak around 0.84 V). The intensive sharp peak in the low potential region is attributed to the reduction of Mn^{2+} to Mn leading to the formation of Li_2O, this peak moves to 0.32 V in other cycles. During the first charge process, the broad anodic peak at 1.27 V can be ascribed to the simultaneous oxidation processes of metallic Mn to Mn^{2+} that cause the Li_2O decomposition (**Figure 10b**). The rate capability of the working electrodes was performed at different current densities as shown in **Figure 10c**. The cell delivers average charge capacities of 377, 310, 273, 235, 180, and 104 mAh g^{-1}, at current rates of C/5, C/4, C/3, C/2, 1C, and 2C respectively with 1C = 1.87 A g^{-1}. When the current density was back to C/5, a charge capacity of 233 mAh g^{-1} was recovered. With a coulombic efficiency of 96, 98, 98, 99, 99, 98, and 99%, respectively.

4. Conclusions

In this chapter, we have reported the potential use of the transition metal oxides (TMOs) as promising anodes for LIBs. TMOs are characterized by their high theoretical capacities, suitable operation voltages, and a variety of chemical compositions. However, their practical use is still limited due to their poor electronic conductivity and high-volume expansion during the Li^+ insertion/extraction. To alleviate these challenges different approaches were suggested:

- The design of three-dimensional (3D) structures with hierarchical configurations,
- The elaboration of the TMOs at the nanometric scale,
- The production of hollow structures,
- The hybridization with carbonaceous materials besides the carbon coating approach.

Here, we have outlined how reducing the particle size to the nanoscale enhances the lithium storage reversibility for the conversion of metal oxides. $Mn_xCo_{3-x}O_4$ $0 \leq x \leq 3$, octahedral-like nanoparticles were prepared by a bio-inspired, cost-effective, and environmentally friendly synthesis method using metal nitrate as a precursor and alginate biopolymer as a sacrificial biotemplate. After a thermal treatment of the organic-inorganic compound at 600°C, the biopolymer degrades and the metal oxides with spinel structure are released. Electrochemical characterization of $Mn_xCo_{3-x}O_4$ $0 \leq x \leq 3$ demonstrated that these materials exhibit high capacities with good capacity retention and rate capability performances, making them potential anode materials for the next generation LIBs.

Acknowledgements

The authors wish to acknowledge Office Chérifien des Phosphates (OCP S.A.) and Mohammed VI Polytechnic University for financial support, and PCM2E laboratory of Tours University.

Author details

Loubna Hdidou[1], Fouad Ghamouss[1,2], Bouchaib Manoun[1,3], Hassan Hannache[1,4], Jones Alami[1] and Mouad Dahbi[1*]

1 Materials Science and Nano-engineering Department, Mohammed VI Polytechnic University, Ben Guerir, Morocco

2 Laboratoire PCM2E (EA 6296), UFR Sciences et Techniques, Université François Rabelais de Tours, Tours, France

3 Hassan First University Rayonnement-Matière et Instrumentation, Settat, Morocco

4 Laboratoire d'Ingénierie et Matériaux (LIMAT), Faculty of sciences Ben M'sik, Hassan II University of Casablanca, Casablanca, Morocco

*Address all correspondence to: mouad.dahbi@um6p.ma

References

[1] Wang Q, Mao B, Stoliarov SI, Sun J. A review of lithium-ion battery failure mechanisms and fire prevention strategies. Progress in Energy and Combustion Science. 2019;**73**:95-131

[2] Stevens DA, Dahn JR. The mechanisms of lithium and sodium insertion in carbon materials. Journal of Electrochemical Society. 2001;**148**(8):A803. DOI: 10.1149/1.1379565

[3] Hassoun J, Bonaccorso F, Agostini M, Angelucci M, Betti MG, Cingolani R, et al. A lithium-ion battery based on a graphene nanoflakes ink anode and a lithium iron phosphate cathode. Nano Letters. 2014;**14**(8):4901-4906

[4] Zhang T, Han S, Guo W, Hou F, Liu J. Continuous carbon nanotube composite fibers for flexible aqueous lithium-ion batteries. Sustainable Materials and Technologies. 2019;**20**:e00096

[5] Yin H, Li Q, Cao M, Zhang W, Zhao H, Li C, et al. Nanosized-bismuth-embedded 1D carbon nanofibers as high-performance anodes for lithium-ion and sodium-ion batteries. Nano Research. 2017;**10**(6):2156-2167

[6] Xue C, Liu Y, Zhao J, Li X, Zhang J, Zhang J. Micro–mesoporous nitrogen-doped hollow carbon nanospheres as anodes for lithium-ion batteries with high-rate capability and outstanding cycling performance. Ceramics International. 2021;**48**:5434-5441

[7] Sun H, Del Rio Castillo AE, Monaco S, Capasso A, Ansaldo A, Prato M, et al. Binder-free graphene as an advanced anode for lithium batteries. Journal of Material Chemistry A. 2016;**4**(18):6886-6895. DOI: 10.1039/C5TA08553E

[8] Hansen S, Quiroga-González E, Carstensen J, Föll H. Size-dependent cyclic voltammetry study of silicon microwire anodes for lithium-ion batteries. Electrochimica Acta. 2016;**217**:283-291

[9] Kang K, Lee H, Han D, Kim G, Lee D, Lee G, et al. Maximum Li storage in Si nanowires for the high-capacity three-dimensional Li-ion battery. Applied Physical Letters. 2010;**96**(5):053110

[10] Wang L, Bao K, Lou Z, Liang G, Zhou Q. Chemical synthesis of germanium nanoparticles with uniform size as anode materials for lithium-ion batteries. Dalton Transactions. 2016;**45**(7):2814-2817. DOI: 10.1039/C5DT04749H

[11] Zhu J, Ding X. A facile one–pot synthesis of Sn/graphite/graphene nanocomposites as anode materials for lithium–ion batteries. Journal of Alloys and Compounds. 2019;**809**:151870

[12] Meng J-K, Fu L, Liu Y, Zheng G, Zheng X, Guan X, et al. Gas-liquid interfacial assembly and electrochemical properties of 3D highly dispersed α-Fe_2O_3@graphene aerogel composites with a hierarchical structure for applications in anodes of lithium ion batteries. Electrochimica Acta. 2017;**224**:40-48

[13] Zheng F, Yin Z, Xia H, Bai G, Zhang Y. Porous MnO@C nanocomposite derived from metal-organic frameworks as anode materials for long-life lithium-ion batteries. Chemical Engineering Journal. 2017;**327**:474-480

[14] Palmieri A, Spinner N, Zhao S, Mustain WE. Explaining the role and mechanism of carbon matrices in enhancing reaction reversibility of metal

oxide anodes for high performance Li ion batteries. Carbon. 2018;**130**:515-524

[15] Varapragasam SJP, Balasanthiran C, Gurung A, Qiao Q, Rioux RM, Hoefelmeyer JD. Kirkendall growth of hollow Mn_3O_4 nanoparticles upon galvanic reaction of MnO with Cu^{2+} and evaluation as anode for lithium-ion batteries. Journal of Physical Chemistry C. 2018;**121**(21):11089-11099

[16] Li ZH, Zhao TP, Zhan XY, Gao DS, Xiao QZ, Lei GT. High capacity three-dimensional ordered macroporous $CoFe_2O_4$ as anode material for lithium ion batteries. Electrochimica Acta. 2010;**55**(15):4594-4598

[17] Duan L, Wang Y, Wang L, Zhang F, Wang L. Mesoporous MFe_2O_4 (M=Mn, Co, and Ni) for anode materials of lithium-ion batteries: Synthesis and electrochemical properties. Materials Research Bulletin. 2015;**61**:195-200

[18] Cheng X, Li Y, Shi H, Lu J, Zhang Y. Rate-dependent electrochemical reaction mechanism of spinel metal oxide anode studied by in situ TEM. Journal of Alloys and Compounds. 2018;**763**:349-354

[19] Boebinger MG, Yeh D, Xu M, Miles BC, Wang B, Papakyriakou M, et al. Avoiding fracture in a conversion battery material through reaction with larger ions. Joule. 2018;**2**(9):1783-1799

[20] Cao K, Jin T, Yang L, Jiao L. Recent progress in conversion reaction metal oxide anodes for Li-ion batteries. Material Chemical Frontiers. 2017;**1**(11):2213-2242. DOI: 10.1039/C7QM00175D

[21] Lu Y, Yu L, David Lou XW. Nanostructured conversion-type anode materials for advanced lithium-ion batteries. Chemistry. 2018;**4**(5):972-996

[22] Park YJ, Lee KS, Shim J, Lee J-H, Kim Y, Son DI. Suppression of volume expansion by graphene encapsulated Co_3O_4 quantum dots for boosting lithium storage. Journal of Industrial and Engineering Chemistry. 2021;**95**:333-339

[23] Singh J, Lee S, Kim S, Singh SP, Kim J, Rai AK. Fabrication of 1D mesoporous NiO nano-rods as high capacity and long-life anode material for lithium ion batteries. Journal of Alloys and Compounds. 2021;**850**:156755

[24] Wang Z, Shi H, Yang S, Cai Z, Lu H, Jia L, et al. Oxygen vacancy-enriched Co_3O_4 as lithiophilic medium for ultra-stable anode of lithium metal batteries. Journal of Alloys and Compounds. 2021;**888**:161553

[25] Kong X, Zhu T, Cheng F, Zhu M, Cao X, Liang S, et al. Uniform $MnCo_2O_4$ porous dumbbells for lithium-ion batteries and oxygen evolution reactions. ACS Applied Material Interfaces. 2018;**10**(10):8730-8738

[26] Wu D, Zhang L, Zhang J, Zhang Z, Liang F, Jiang L, et al. Novel self-supporting multilevel-3D porous NiO nanowires with metal-organic gel coating via "like dissolves like" to trigger high-performance binder-free lithium-ion batteries. Microporous and Mesoporous Materials. 2021;**328**:111483

[27] Augustin M, Fenske D, Bardenhagen I, Westphal A, Knipper M, Plaggenborg T, et al. Manganese oxide phases and morphologies: A study on calcination temperature and atmospheric dependence. Beilstein Journal of Nanotechnology. 2015;**6**:47-59

[28] Li D, Yang D, Zhu X, Jing D, Xia Y, Ji Q, et al. Simple pyrolysis of cobalt alginate fibres into Co_3O_4 /C nano/microstructures for a high-performance lithium ion battery anode. Journal of Materials Chemistry A. 2014;**2**(44):18761-18766

[29] Koo B, Xiong H, Slater MD, Prakapenka VB, Balasubramanian M, Podsiadlo P, et al. Hollow iron oxide nanoparticles for application in lithium ion batteries. Nano Letters. 2012;**12**(5):2429-2435

[30] Jian G, Xu Y, Lai L-C, Wang C, Zachariah MR. Mn_3O_4 hollow spheres for lithium-ion batteries with high rate and capacity. Journal of Material Chemistry A. 2014;**2**(13):4627-4632. DOI: 10.1039/C4TA00207E

[31] Karunakaran G, Kundu M, Maduraiveeran G, Kolesnikov E, Gorshenkov MV, Balasingam S, et al. Hollow mesoporous heterostructures negative electrode comprised of $CoFe_2O_4$@Fe_3O_4 for next generation lithium-ion batteries. Microporous and Mesoporous Materials. 2018;**272**:1-7

[32] Xie Y, Qiu Y, Tian L, Liu T, Su X. Ultrafine hollow Fe_3O_4 anode material modified with reduced graphene oxides for high-power lithium-ion batteries. Journal of Alloys and Compounds. 2022;**894**:162384

[33] Wu L, Xiao Q, Li Z, Lei G, Zhang P, Wang L. $CoFe_2O_4$/C composite fibers as anode materials for lithium-ion batteries with stable and high electrochemical performance. Solid State Ionics. 2012;**215**:24-28

[34] Li S, Wang B, Liu J, Yu M. In situ one-step synthesis of $CoFe_2O_4$/graphene nanocomposites as high-performance anode for lithium-ion batteries. Electrochimica Acta. 2014;**129**:33-39

[35] Wang L, Zheng Y, Wang X, Chen S, Xu F, Zuo L, et al. Nitrogen-doped porous carbon/Co_3O_4 nanocomposites as anode materials for lithium-ion batteries. ACS Applied Materials Interfaces. 2014;**6**(10): 7117-7125

[36] Hdidou L, Khallouk K, Solhy A, Manoun B, Oukarroum A, Barakat A. Synthesis of CoFeO mixed oxides *via* an alginate gelation process as efficient heterogeneous catalysts for lignin depolymerization in water. Catalysis Science Technology. 2018;**8**(21):5445-5453. DOI: 10.1039/C8CY00576A

[37] Xing X, Liu R, Liu S, Xiao S, Xu Y, Wang C, et al. Surfactant-assisted hydrothermal synthesis of cobalt oxide/nitrogen-doped graphene framework for enhanced anodic performance in lithium-ion batteries. Electrochimica Acta. 2016;**194**:310-316

[38] Zhang L, He G, Lei S, Qi G, Jiu H, Wang J. Hierarchical hollow microflowers constructed from mesoporous single crystalline $CoMn_2O_4$ nanosheets for high performance anode of lithium ion battery. Journal of Power Sources. 2016;**326**:505-513

[39] Luo Y, Chen C, Chen L, Zhang M, Wang T. 3D reticular pomegranate-like $CoMn_2O_4$/C for ultrahigh rate lithium-ion storage with re-oxidation of manganese. Electrochimica Acta. 2017;**241**:244-251

[40] Wang M, Huang Y, Zhang N, Wang K, Chen X, Ding X. A facile synthesis of controlled Mn_3O_4 hollow polyhedron for high-performance lithium-ion battery anodes. Chemical Engineering Journal. 2018;**334**:2383-2391

[41] Pan X, Ma J, Yuan R, Yang X. Layered double hydroxides for preparing $CoMn_2O_4$ nanoparticles as anodes of lithium-ion batteries. Materials Chemistry and Physics. 2017;**194**:137-141

[42] Yan J, Zhang J, Su Y-C, Zhang X-G, Xia B-J. A novel perspective on the formation of the solid electrolyte interphase on the graphite electrode for lithium-ion batteries. Electrochimica Acta. 2010;**55**(5):1785-1794